



1 **Enhanced upward motion through the troposphere over the tropical**
2 **western Pacific and its implication to transport of trace gases from**
3 **the troposphere to the stratosphere**

4 Kai Qie ¹, Wuke Wang², Wenshou Tian ^{1*}, Rui Huang¹, Mian Xu¹, Tao Wang¹,

5 Yifeng Peng¹

6

7 ¹*College of Atmospheric Sciences, Lanzhou University, Lanzhou 730000, China*

8 ²*Department of Atmospheric Science, China University of Geosciences, Wuhan*
9 *430074, China*

10

11

12 *Corresponding author: Wenshou Tian (wstian@lzu.edu.cn)

13



14 **Abstract**

15 The tropical western Pacific (TWP) is a preferential area of air uplifting from the
16 surface to the upper troposphere. A significantly intensified upward motion through
17 the troposphere over the TWP in the boreal wintertime (November to March of the
18 next year) has been detected from 1958 to 2017 using the reanalysis datasets. Model
19 simulations using the Whole Atmosphere Community Climate Model, version 4
20 (WACCM4) suggest that warming global sea surface temperatures (SSTs),
21 particularly TWP SSTs, play a dominant role in the intensification of the upward
22 motion by strengthening the Pacific Walker circulation and enhancing the deep
23 convection over the TWP. Using CO as a tropospheric tracer, numeric simulations
24 show that more CO could be elevated to the tropical tropopause layer (TTL) by the
25 enhanced upward motion over the TWP and subsequently into the stratosphere by the
26 strengthened Brewer-Dobson (BD) circulation which is also mainly caused by global
27 SST warming. This implies that more tropospheric trace gases and aerosols may enter
28 the stratosphere through the TWP region and affect the stratospheric chemistry and
29 climate.

30 **Keywords:** Troposphere-to-stratosphere transport; Tropical western Pacific; Trend;
31 Sea surface temperature

32



33

34 **1 Introduction**

35 The tropical western Pacific (TWP) is a critical region for tropical and global
36 climate (e.g., Webster et al., 1996; Hu et al., 2020). It has the largest area of warm sea
37 surface temperature (exceeding 28 °C) which fuels intense and massive deep
38 convection and thus is the largest source of latent heat and water vapor into the
39 atmosphere (Webster and Lukas, 1992). The TWP region is also the most important
40 source of tropospheric air entering the stratosphere due to the strong upward motion
41 and deep convection over this region (e.g., Fueglistaler et al., 2004; Pan et al., 2016).
42 Through the TWP region, tropospheric trace gases, e.g., the organic halogen species,
43 are elevated from the surface to the upper troposphere and lower stratosphere, which
44 affects the ozone concentration and other chemical processes in the stratosphere
45 (Saiz-Lopez and von Glasow, 2012; Wang et al., 2015). At the same time, the TWP
46 region has the coldest tropopause and plays an important role in controlling the water
47 vapor concentration in the stratosphere (e.g., Fueglistaler et al., 2009; Newell and
48 Gould-Steward, 1981; Pan et al., 2016; Randel and Jensen, 2013). Hence, the TWP is
49 also an important region for troposphere-to-stratosphere transport and stratospheric
50 chemistry.

51 The TWP was thought to be the main pathway of the troposphere-to-stratosphere
52 transport. A concept of “stratospheric fountain” was proposed by Newell and
53 Gould-Steward (1981), which suggested that the poor-water vapor air in the
54 stratosphere stems mainly from the TWP region. However, following studies using the



55 observational and reanalysis data showed that there is subsidence at the
56 near-tropopause level over the maritime continent, which is named as the
57 “stratospheric drain” (Gettelman et al., 2000; Sherwood, 2000; Fueglistaler et al.,
58 2004). Further studies verified that the large-scale transport from the tropical
59 tropopause layer (TTL) to the stratosphere is dominated by the upward branch of the
60 Brewer-Dobson (BD) circulation (Brewer, 1949; Dobson, 1956; Holton et al., 1995)
61 while the local upwelling may play a minor role (e.g., Levine et al., 2007; Fueglistaler
62 et al., 2009; Schoeberl et al., 2018).

63 Though the TWP is not the dominant entry of trace gases transported from the
64 troposphere into the lower stratosphere, numerous studies confirmed that the TWP
65 region is an important pathway of the surface air entering the TTL (Fueglistaler et al.,
66 2004; Levine et al., 2007; Krüger et al., 2008; Haines and Esler, 2014). The very short
67 lived substances, which play an important role in regulating the ozone concentration,
68 could be elevated to the TTL by the strong upward motion and the deep convection
69 over the TWP and subsequently into the stratosphere by the large-scale upwelling
70 (e.g., Levine et al., 2007, 2008; Navarro et al., 2015). Based on a trajectory model,
71 Fueglistaler et al. (2004) pointed out that the TWP region is a primary source of the
72 tropospheric air entering the stratosphere and approximately 80% of the trajectories
73 ascending into the stratosphere enter the TTL from the TWP. Bergman et al. (2012)
74 suggested that the tropospheric air over the TWP enters the stratosphere mainly in
75 boreal winter, while less air over the TWP could be transported into the stratosphere
76 during boreal summer. Other studies also found that the TWP region is an important



77 source of the tropospheric trace gases in the TTL (e.g., Newton et al., 2018; Pan et al.,
78 2016; Wales et al., 2018), even the polluted air from East Asia could be transported
79 rapidly to Southeast Asia by meridional winds and subsequently be elevated to the
80 tropical upper troposphere by the strong upward motion and the deep convection
81 (Ashfold et al., 2015). Hence, the strength of the upward motion over the TWP region
82 during boreal winter is a key feature for understanding the variations of trace gases in
83 the TTL and therefore important for stratospheric chemistry and climate.

84 The strength of the TWP upward motion is closely related to atmospheric
85 circulation and deep convection. The ascending branch of the Pacific Walker
86 circulation and the strong deep convection over the TWP allow rapid transport from
87 the surface to the upper troposphere (Hosking et al., 2012). In association with global
88 warming, atmospheric circulation, deep convection as well as the boundary conditions
89 (e.g., sea surface temperature; SST) have been changed. For example, the Hadley cell
90 has been extended to the subtropics and the Walker circulation over the Pacific has
91 been shifted westward over the past decades (e.g., Lu et al., 2007; Garfinkel et al.,
92 2015; Ma and Zhou, 2016). At the same time, SSTs over most of areas are getting
93 warmer (Cane et al., 1997; Deser et al., 2010), which modulates the deep convection
94 and atmospheric wave activities in the troposphere and then lead to changes of
95 atmospheric circulations from the troposphere and the stratosphere (e.g., Garfinkel et
96 al., 2013; Xie et al., 2012, 2014a; Wang et al., 2015; Hu et al., 2016; Lu et al., 2020).
97 However, how the strength of the upward motion in the lower TTL over the TWP
98 region has been changed over the past decades remains unclear. In this study, we



99 investigate the long-term trend of the upward motion over the TWP using reanalysis
100 datasets and model simulations. The implication of the changes in the upward motion
101 over the TWP to the transport of trace gases from the surface to the upper troposphere
102 and lower stratosphere is also discussed.

103 **2 Data and method**

104 **Reanalysis data.** Three reanalysis datasets, including JRA55, ERA5 and
105 MERRA2 are used in this study. The Japanese 55-year Reanalysis (JRA55) is
106 conducted by the Japan Meteorological Agency (JMA). JRA55 is produced by an
107 atmospheric model with higher spatial resolution (T319L60), using a four
108 dimensional variational (4D-Var) data assimilation system. It has a horizontal
109 resolution of $1.25^{\circ} \times 1.25^{\circ}$, and covers the period from 1958 to present (Kobayashi et
110 al., 2015; Harada et al. 2016). The ERA5 reanalysis is the newest generation product
111 from the European Centre for Medium Range Weather Forecasting (Hersbach et al.,
112 2020). The ERA5 data also extend back to 1958, which is coinciding with the time
113 that radiosonde observations in the Arctic became more systematic and regular. It
114 should be noted that the ERA5 data suffers from a bias during 2000-2006, and is
115 replaced by the ERA5.1 data in this period here. The Modern-Era Retrospective
116 analysis for Research and Applications version 2 (MERRA2; $1.25^{\circ} \times 1.25^{\circ}$ horizontal
117 mesh) dataset are also used, which is only accessible after 1980 (Gelaro et al., 2017).
118 The monthly mean air temperature, horizontal wind fields and vertical velocity at
119 different pressure levels are extracted from the three Reanalysis data sets. The
120 accuracy of the vertical velocity in reanalysis data sets has been evaluated by the



121 Reanalysis Intercomparison Project (Fujiwara et al., 2017), which is initiated by the
122 Stratosphere-troposphere Processes And their Role in Climate (SPARC). Results of a
123 comparison between the radar observed data and the reanalysis data indicate that the
124 updrafts in the UTLS are captured well near the TWP even though there are still large
125 biases in the reanalysis datasets (Uma et al. 2021). Hitchcock (2019) suggested that
126 the reanalysis uncertainty is larger in the radiosonde era (after 1958) than in the
127 satellite era (after 1979), but the radiosonde era is of equivalent value to the satellite
128 era because the dynamical uncertainty dominates in the both eras. Hence, the present
129 study investigate the long-term trend of the upward motion over the TWP from 1958
130 to 2017.

131 **SST and OLR data.** The SST data is from the HadISST dataset ($1^{\circ}\times 1^{\circ}$
132 horizontal mesh) during 1958-2018 (Rayner et al., 2003). The outgoing longwave
133 radiation (OLR), which is utilized to reflect the deep convection in the tropics, is
134 extracted from NOAA Interpolated OLR dataset on a $2.5^{\circ}\times 2.5^{\circ}$ horizontal mesh
135 during 1974/11-2018/03 (Liebmann and Smith, 1996).

136 **Model simulations.** A series of the Whole Atmosphere Community Climate
137 Model version 4 (WACCM4) simulations are performed to find out the main impact
138 factors of the trend of the upward motion over the TWP. The WACCM4 used in this
139 study is an atmosphere-only model with a horizontal resolution of $1.9^{\circ}\times 2.5^{\circ}$, which
140 has a vertical resolution of 66 vertical levels (Marsh et al., 2013). A hindcast
141 simulation (Control run) is performed with observed greenhouse gases, solar
142 irradiances, and prescribed SSTs (HadISST dataset is used) during 1955-2018. A



143 single-factor controlling run (Fixsst run) is done for the same period with the same
144 forcings, except that the global SSTs are fixed to the climatological mean values
145 during 1955-2018 (long-term mean for each calendar month during 1955-2018). A
146 couple of time-slice simulations are also integrated for 33 years to investigate the
147 impact of the SST over the TWP region on the trend of the upward motion over the
148 TWP. The SSTs of both simulations are prescribed as the climatological mean SST
149 during 1958-2017, while the SST anomalies over the tropical western Pacific
150 (20°S-20°N, 120°E-160°E) in the boreal wintertime (November to March of the next
151 year, NDJFM) during 1998-2017 are added to one (R1) simulation and SST anomalies
152 over the tropical western Pacific (20°S-20°N, 120°E-160°E) in NDJFM during
153 1958-1977 are added to the other simulation (R2). The first 3 years of the numeric
154 simulations are not used in the present study to provide a spin-up.

155 **Transformed Eulerian Mean (TEM) Calculation.** To diagnose the changes in
156 the BD circulation, the meridional and vertical velocities of the BD circulation are
157 calculated by the TEM equations (Andrews and McIntyre, 1976):

$$158 \quad \bar{v}^* = \bar{v} - \frac{1}{\rho} \left(\frac{\overline{\rho v' \theta'}}{\theta_z} \right)_z$$
$$159 \quad \bar{w}^* = \bar{w} + \frac{1}{a \cos \varphi} \left(\cos \varphi \frac{\overline{v' \theta'}}{\theta_z} \right)_\varphi$$

160 Where \bar{v}^* and \bar{w}^* denote the meridional and vertical velocities of the BD circulation;
161 the overbar represents the zonal mean; the prime denotes the deviation from the zonal
162 mean; θ , a , φ , and ρ indicate the potential temperature, the radius of the earth,
163 the latitude, and the standard density.



164 **3 Results**

165 **3.1 Enhanced upward motion over the TWP**

166 According to previous studies, the lapse-rate tropopause is a good proxy to
167 separate the tropospheric and the stratospheric dynamic behavior (vertical motion
168 dominated and horizontal mixing dominated, respectively) over the TWP (Pan et al.,
169 2019). Since the lapse-rate tropopause over the TWP in the boreal winter is near 100
170 hPa (not shown), we utilize the vertical velocity at 150 hPa to reflect the vertical
171 transport in the upper troposphere. Figure 1 shows the climatological distribution of
172 the vertical velocity at 150 hPa for each month of the year. The TWP region at the
173 UTLS level has strong upward motion due to the frequent intense deep convection
174 and the Pacific Walker circulation. It is noteworthy that there is strong upward motion
175 at 150 hPa in NDJFM over the TWP, while the upward motion in other months shifts
176 northward corresponding to the Asia summer monsoon. This is consistent with
177 previous studies (Newell and Gould-Steward, 1981; Bergman et al., 2012). Therefore,
178 we mainly focus on the changes in the upward motion in NDJFM, which is more
179 important to the transport of air over the TWP from the lower troposphere to the TTL
180 and subsequently to the lower stratosphere. The 150 hPa vertical velocity (w) shows
181 positive values over the TWP, which are almost symmetry along the equator in
182 NDJFM (Fig. 1). Notably, the 150 hPa w shows no subsidence over the maritime
183 continent, while there is descending motion over the maritime continent at 100 hPa
184 (not shown), which is referred to the “stratospheric drain” (Gettleman et al., 2000;
185 Sherwood, 2000).



186 Figure 2 displays the linear trends of w in the upper (150 hPa), middle (500 hPa)
187 and lower (700 hPa) troposphere in NDJFM from 1958 to 2017 using three reanalysis
188 datasets. The 150 hPa w increased significantly over the TWP during 1958-2017 (Fig.
189 2). Additionally, the upward motion over the TWP in the lower and middle
190 troposphere also shows significantly intensifying trends (Figs. 2b and c). This
191 indicates that the upward motion over the TWP is intensifying through the
192 troposphere. Such an enhancement of the upward motion over the TWP is evident in
193 all three reanalysis datasets (JRA55, ERA5, and MERRA2).

194 The time series of the upward motion intensity over the TWP (vertical velocity
195 averaged for the region 20°S-10°N, 100°E-180°E) from different datasets are given in
196 Fig. 3. The intensity of the upward motion over the TWP at 150 hPa increases
197 significantly in NDJFM during last decades, which can be confirmed by all the three
198 reanalysis data (Fig. 3). The intensity of the upward motion over the TWP in the
199 lower and middle troposphere is also enhanced significantly (Figs. 3b and c). This
200 suggests a comprehensive enhancement of vertical velocity though the whole
201 troposphere, which is evident from the surface to 100 hPa (not shown). While the
202 trace gases in the TTL are modulated by the upward motion and subsequent vertical
203 transport (e.g., Garfinkel et al., 2013; Xie et al., 2014b), such a strengthening of the
204 upward motion over the TWP may lead to the more tropospheric trace gases in the
205 TTL. Due to the data limitation, it is not possible to show the corresponding changes
206 of trace gases by observations. However, we will discuss the CO changes by model
207 simulations in section 3.3.



208 The changes in the atmospheric circulation at the UTLS level in the tropics are
209 closely related to the changes in the tropical deep convection and SSTs (e.g., Levine
210 et al., 2008; Garfinkel et al., 2013; Xie et al., 2020). Here, the trends of observed OLR
211 in NDJFM during 1974-2017 are shown in Fig. 4a. Though the time period of the
212 observed OLR data is shorter than the time period we analyzed, the changes in OLR
213 could partly reflect the changes in the deep convection during 1958-2017. The OLR
214 shows significantly negative trends over the TWP which indicates intensified deep
215 convection over the TWP. The OLR trend pattern is very similar to the trend pattern
216 of the 150 hPa w (Figs. 2a-c), which indicates that the increasing trends of 150 hPa w
217 are closely related to the intensified deep convection over the TWP. The intensified
218 deep convection not only lead to the strengthened upward motion in the UTLS
219 (Highwood and Hoskins, 1998; Ryu and Lee, 2010), but also result in the decreased
220 temperature near the tropopause which plays a dominant role in modulating the lower
221 stratospheric water vapor concentration (e.g., Hu et al., 2016; Wang et al., 2016).
222 Corresponding to the enhanced deep convection over the TWP, the CPTT shows
223 significantly decreasing trends over the TWP in NDJFM during 1958-2017, which is
224 consistent with Xie et al., (2014a).

225 The changes in the deep convection over the tropical Pacific may be related to
226 the changes in the Pacific Walker circulation. The Pacific Walker circulation shows a
227 significant intensification over the past decades (e.g., Meng et al., 2012; L'Heureux et
228 al., 2013; McGregor et al., 2014). The vertical velocity at 500 hPa and 150 hPa shows
229 significantly positive trends over the TWP in NDJFM during 1958-2017 (Fig. 2).



230 Meanwhile, the lower tropospheric zonal wind shows easterly trends over the tropical
231 Pacific, while the upper tropospheric zonal wind shows westerly trends over the
232 tropical Pacific, which suggests a strengthened Pacific Walker circulation and is
233 consistent with previous studies (Hu et al., 2016; Ma and Zhou, 2016).

234 The strengthened Pacific Walker circulation is closely related to the changes in
235 the SSTs (e.g., Meng et al., 2012; Ma and Zhou, 2016). The trends of the SSTs in
236 NDJFM during 1958-2017 are shown in Fig. 4c. The SST shows significantly
237 warming trends almost over the world except the central Pacific in NDJFM during
238 1958-2017. In addition, the intensity of the upward motion over the TWP is
239 significantly correlated with the SST (Fig. 4d), which suggests that the SST has
240 important effects on the upward motion over the TWP. The correlation coefficient in
241 Figure 4d shows a La Niña-like pattern and indicates that the ENSO events exert
242 important impacts on the upward motion over the TWP (Levine et al., 2008). The
243 SSTs over the TWP are positively correlated with the upward motion intensity over
244 the TWP, while the SSTs over tropical central, eastern Pacific, and Indian Ocean show
245 negative correlations with the intensity of the upward motion over the TWP. The SSTs
246 over the Atlantic Ocean are poorly correlated with the upward motion intensity over
247 the TWP (not shown). This result suggests that the changes in global SSTs may be the
248 primary driver of the strengthened Pacific Walker circulation, which leads to
249 enhanced deep convection and intensified upward motion over the TWP.

250 **3.2 Simulated trend of the upward motion over the TWP and its potential**
251 **mechanism**



252 To verify the impact of SST on the trend of the upward motion over the TWP, a
253 couple of model simulations are employed in the following analysis. Consistent with
254 the results shown using the reanalysis data (Figs. 2a-c), the simulated 150 hPa w
255 (Control run) shows significantly increasing trends over the TWP and decreasing
256 trends over the tropical eastern Pacific in NDJFM during 1958-2017 (Fig. 5a).
257 Additionally, the 150 hPa w simulated in the Fixsst run shows weak trends over the
258 TWP (Fig. 5b). The difference between the control and the Fixsst runs suggests that
259 the trends of the 150 hPa w over the TWP region is dominated by the changes in the
260 global SSTs during 1958-2017. There are also significantly positive trends of the
261 vertical velocity over the TWP in the lower (700 hPa) and middle troposphere (500
262 hPa) in the Control run, while the zonal winds are also enhanced over the tropical
263 Pacific. The vertical velocity over the TWP in the Fixsst run shows weak negative
264 trends and the changes in zonal winds over the tropical Pacific are very weak. This
265 confirms the dominant role of the changes in global SSTs on the enhancement of the
266 Walker circulation.

267 Previous studies found that the changes in the intensity of the Pacific Walker
268 circulation and the stratospheric residual circulation are closely related to the changes
269 in tropical SST (Meng et al., 2012; Tokinaga et al., 2012; Lin et al., 2015). As the
270 SSTs over tropical central and eastern Pacific, and Indian Ocean, show negative
271 correlations with the intensity of the upward motion over the TWP in the lower TTL
272 (Fig. 2f), the warming trends of SSTs over these regions may lead to a weakened
273 upward motion over the TWP. Hence, the warming trends of the SSTs over the TWP



274 may be the main factor causing the intensification of the upward motion over the TWP.
275 To verify the impact of the changes in the SSTs over the TWP region on the trends of
276 the upward motion over the TWP, a couple of time-slice runs (R1 and R2) are
277 performed (more details are given in the section 2). The differences of the wind fields
278 between R1 and R2 are shown in Fig. 6. The 150 hPa w shows significantly positive
279 anomalies over the TWP and negative anomalies over the tropical eastern Pacific,
280 which is consistent with the trends of the 150 hPa w in the Control run and the
281 reanalysis datasets (Figs. 2 and 5). The upward motion in the lower and middle
282 troposphere over the TWP shows intensifying trends due to the enhanced convergence
283 induced by the warmer SSTs over the TWP. This result is consistent with Hu et al.
284 (2016), which suggested that the increased zonal gradient of the SSTs over the
285 tropical Pacific could lead to a strengthened Pacific Walker circulation and an
286 enhanced upward motion over the TWP. Therefore, the warmer SSTs over the TWP
287 could contribute largely to the trend of the upward motion over the TWP in NDJFM
288 during 1958-2017.

289 The changes in the OLR associated with the changes in the global SSTs are
290 shown in Fig. 7. There are significantly enhanced deep convection as indicated by
291 OLR over the TWP due to the strengthened convergence in the Control run, while the
292 deep convection show weak and even decreasing trends over the TWP in the Fixsst
293 run (Figs. 7a and 7b). The enhanced deep convection over the TWP could lead to the
294 enhancing trends of the upward motion. Hence, it can be inferred that the changes in
295 the global SSTs are responsible for the intensification of the Pacific Walker circulation,



296 and the enhanced deep convection and a stronger upward motion over the TWP which
297 could extend to the upper troposphere.

298 **3.3 Implications to the concentrations of water vapor and CO in the TTL**
299 **and lower stratosphere.**

300 We now discuss about the relationship between the trends of the upward motion
301 over the TWP and the changes of the trace gases in the lower stratosphere. The trends
302 of CPTT, the 100 hPa streamfunction, and the water vapor concentration in different
303 simulations are displayed in Fig. 7. The changes in the deep convection could lead to
304 the changes in the atmospheric circulation by releasing the latent heat. The changes in
305 the tropical deep convection lead to a Rossby-Kelvin wave response at the UTLS
306 level and then induce the changes in the air temperature near the tropopause (e.g., Gill,
307 1980; Highwood and Hoskins, 1998). The trends of the 100 hPa streamfunction show
308 a Rossby wave response over the TWP and a Kelvin wave response over the tropical
309 eastern Pacific in the Control run (Fig. 7d), which is caused by the changes in the
310 deep convection over the tropical Pacific. The Rossby-Kelvin wave response further
311 leads to the decreasing trends of the CPTT over the TWP and the increasing trends of
312 the CPTT over the tropical eastern Pacific. Previous studies suggest that the lower
313 stratospheric water vapor is mainly influenced by the coldest temperature near the
314 tropopause (e.g., Garfinkel et al., 2018; Zhou et al., 2021). Since the TWP has the
315 coldest CPTT in the boreal winter (e.g., Pan et al., 2016), the significantly decreased
316 CPTT over the TWP may result in significantly dried lower stratosphere (Fig. 7g).
317 The intensity of the upward motion over the TWP shows negative correlations with



318 the concentration of the tropical lower stratospheric water vapor (not shown). Hence,
319 the enhanced upward motion over the TWP may correspond to a dried lower
320 stratosphere. The CPTT shows weak trends over the TWP, and the tropical water
321 vapor shows insignificant trends at 70 hPa in the Fixsst run. The comparison between
322 the Control run and the Fixsst run suggests that the trends of the deep convection, the
323 CPTT, and the lower stratospheric water vapor concentration in the tropics in NDJFM
324 during 1958-2017 are dominated by the trends of the global SSTs, while other
325 external forcings may play minor roles.

326 Generally, the intensified tropical upwelling may lead to more tropospheric trace
327 gases entering the stratosphere (e.g., Rosenlof, 2003). As mentioned above in section
328 3.1, the observed tracer gases (e.g., CO) have very limited data record and may be
329 affected by a mixture of anthropogenic and natural (e.g., biomass burning) emissions
330 and the ENSO events (e.g., Duncan et al., 2007; Logan et al., 2008). It is therefore
331 very hard to identify the relative contribution of single factors. Here, we utilize the
332 numeric simulations to verify the impact of the strengthened upward motion due to
333 the changes in the global SSTs on the concentrations of the trace gases in the TTL
334 over the TWP. The trends of the CO concentration, which acts as a tropospheric tracer
335 are shown in Fig. 8. The tropical CO at 150 hPa shows significantly increasing trends
336 both in the Control run and the Fixsst run (Figs. 8a and 8b), which suggests that the
337 surface emission of the CO exerts an important effect on the increasing trends of the
338 tropical CO concentration. At the same time, the differences of the CO trends at 150
339 hPa between the Control run and the Fixsst run are also displayed in Fig. 8c. Since the



340 surface emission inventories of the two simulations are the same, it can be inferred
341 that the trends of the CO concentration in Fig. 8c are mainly caused by the changes in
342 the atmospheric circulation induced by the changes in the global SSTs. The difference
343 of the CO concentration at 150 hPa between the Control run and the Fixsst run shows
344 significantly increasing trends over the TWP and decreasing trends over the central
345 Africa, which resembles the trend patterns of the vertical velocity in the lower TTL
346 and the deep convection (Figs. 5i and 7c). This indicates that the enhanced deep
347 convection in the TWP lead to the strengthened upward motion over the TWP, which
348 results in more CO in the upper troposphere over the TWP. It could also be found that
349 CO also increases in the mid latitudes of the southern hemisphere (Fig. 8c). According
350 to previous studies, the CO perturbation from the Indonesian fires at upper
351 troposphere could be transported to the tropical Indian Ocean by easterly winds and
352 then to the subtropics in the southern hemisphere through the southward flow during
353 boreal winter. The CO perturbation then spreads rapidly circling the globe following
354 the subtropical jet (Duncan et al., 2007). This is consistent with our results which
355 show intensified northerlies over the subtropical Indian Ocean and strengthened
356 westerlies over the subtropical Indian Ocean and western Pacific (Figs. 5c and f).

357 The trends of the zonal mean CO concentration from model simulations are
358 displayed in Figs. 9a-c. The zonal mean CO shows significantly increasing trends at
359 all levels in the Control run and the Fixsst run, while the difference of the zonal mean
360 CO between the Control run and the Fixsst run shows significantly increasing trends
361 in the TTL but negative trends in the middle troposphere in the tropics and the



362 Northern Hemisphere. At the same time, the difference of CO concentration between
363 the Control run and the Fixsst run averaged in the western Pacific (100°E-180°E)
364 shows significantly increasing trends in the tropics (20°S-10°N) from the surface to
365 the TTL (Fig. 9f). This indicates that the increased zonal mean CO in the TTL (Fig. 9c)
366 is mainly transported through the western Pacific bands. This highlights the
367 importance of the upward motion over the TWP in elevating trace gases from the
368 surface to the upper troposphere.

369 To understand the CO trends in the Control and Fixsst simulations and their
370 differences, the trends of vertical velocity averaged over the globe and the TWP band
371 are given in Fig. 10. The zonal mean w shows weak and even decreasing trends in the
372 tropics while the w over the TWP increases in the control run. This is consistent with
373 Fig. 5. While the SSTs fixed to climatological values, the zonal mean w shows weak
374 trends and the w over the TWP shows significantly decreasing trends. The changes in
375 the global SSTs therefore leads to the increase of the w over the TWP region as
376 indicated in the differences between the two simulations in Fig. 10f. In summary, the
377 increase of CO as shown in Figs. 8a-8b is mainly caused by surface emissions.
378 Enhanced tropospheric upward motion over the TWP forced by the changes in the
379 global SSTs, however, leads to some extra increase of CO concentrations in the upper
380 troposphere.

381 As discussed in the Introduction, the tropospheric trace gases enters the
382 stratosphere mainly through the large-scale tropical upwelling associated with the BD
383 circulation. The trends of the BD circulation in different model simulations as well as



384 their differences are displayed in Fig. 11. The tropical upwelling of BDC (w^*) are
385 significantly increased in the lower stratosphere over past decades as seen in both
386 reanalysis data and the control run (Figs. 11a and b). This is consistent with previous
387 studies (e.g., Rao et al., 2019; Diallo et al., 2021). In the Fixsst run, the trend of w^* is
388 much weaker and not significant in most areas. The changes in the global SSTs
389 therefore play an important role in the intensification of the shallow branch of the
390 BDC as shown by the differences between the two simulations in Fig. 11d. Such
391 strengthened tropical upwelling transports more CO from the upper troposphere to the
392 lower stratosphere as seen in Fig. 9. At the same time, an enhancement of the shallow
393 branch of the BDC also means a stronger meridional transport that contributes to the
394 increase of CO concentration in the subtropics (Fig. 9f). The enhancement of upward
395 motion over the TWP, which transported more tropospheric trace gases to the upper
396 troposphere, works together with the strengthened BD circulation under global
397 warming may lead to an increase of tropospheric trace gases over the TWP in the
398 lower stratosphere.

399 **4 Summary and Discussion**

400 The recent trends of the upward motion from the lower to the upper troposphere
401 in boreal winter over the TWP is investigated for the first time based on the reanalysis
402 datasets and model simulations. An intensified upward motion over the TWP in
403 NDJFM from 1958 to 2017 is detected from both the reanalysis datasets and the
404 model simulations. The trend of the upward motion over the TWP is closely related to
405 the changes in global SSTs, especially the TWP SST warming. Warmer SSTs over the



406 TWP lead to a strengthened Pacific Walker circulation, enhanced deep convection and
407 stronger upward motion over the TWP. The enhanced deep convection over the TWP
408 could lead to a dryer lower stratosphere over the TWP, as the strong upward motion
409 and the Rossby-Kelvin wave responses induce a colder tropopause over the TWP.

410 Model simulations indicate that the CO concentration increases significantly
411 from the surface to the stratosphere with increased surface emissions. However, an
412 enhancement of tropospheric upward motion and subsequent upward transport of
413 trace gases over the TWP leads to some extra increase of CO concentrations in the
414 upper troposphere. The elevated CO in the upper troposphere is further uplifted to the
415 lower stratosphere by the intensified shallow branch of the BD circulation due mainly
416 to global SST warming and lead to an increase of CO in the lower stratosphere.

417 Trace gases and aerosols in the stratosphere have important impacts on the
418 stratospheric processes, and hence influence the tropospheric weather and climate
419 through their radiative and dynamical feedback. Our results suggest that the upward
420 motion over the TWP and the vertical component of the BDC at the lower
421 stratosphere level have been intensified. These results suggest that the emission from
422 the maritime continent may play a more important role in the stratospheric processes
423 and the global climate. In addition, more very short lived substances emitted from the
424 tropical ocean could be elevated to the TTL by the enhanced convection and then
425 transported into the stratosphere by the large-scale uplifts and exert important effects
426 on the stratospheric chemistry. However, the quantitative impacts of the intensified
427 upward motion over the TWP on tropospheric and stratospheric trace gases and



428 aerosols and their climate feedbacks await further investigation using more
429 observations and model simulations.

430

431 **Competing interests.** The authors declare that they have no conflict of interest.

432

433 **Author contributions.** WT designed the study. WW provided suggestions about the
434 statistical methods and model simulations. KQ ran the models and wrote the first draft.
435 RH, MX, and TW contributed to the manuscript writing. YP provided the data used in
436 the study. All authors contributed to the improvement of the results.

437

438

439 **Acknowledgements.** This research is supported by Strategic Priority Research
440 Program of Chinese Academy of Sciences (XDA17010106), the National Natural
441 Science Foundation of China (42075055) and the Supercomputing Center of Lanzhou
442 University. The authors gratefully acknowledge the JRA55 data
443 (<http://rda.ucar.edu/datasets/ds628.0/>). The SST data is obtained from HadISST
444 (<https://www.metoffice.gov.uk/hadobs/hadisst/data/download.html>). The ERA5 data
445 and ERA5.1 data are extracted from
446 <https://cds.climate.copernicus.eu/#!/search?text=ERA5&type=dataset>. And MERRA2
447 data are downloaded from
448 <https://search.earthdata.nasa.gov/search?q=MERRA2&fst0=Atmosphere>,
449 respectively. The OLR data are from
450 https://psl.noaa.gov/data/gridded/data.interp_OLR.html.

451



452 **References:**

- 453 Andrews, D. G., and McIntyre, M. E.: Planetary waves in horizontal and vertical shear:
454 the generalized Eliassen-Palm relation and the mean zonal acceleration, *J. Atmos.*
455 *Sci.*, 33, 2031 – 2048, 1976
- 456 Ashfold, M. J., Pyle, J. A., Robinson, A. D., Meneguz, E., Nadzir, M. S. M., Phang, S.
457 M., Samah, A. A., Ong, S., Ung, H. E., Peng, L. K., Yong, S. E., and Harris, N. R.
458 P.: Rapid transport of East Asian pollution to the deep tropics, *Atmos. Chem.*
459 *Phys.*, 15, 3565-3573, doi:10.5194/acp-15-3565-2015, 2015.
- 460 Bergman, J. W., Jensen, E. J., Pfister, L., and Yang, Q.: Seasonal differences of
461 vertical-transport efficiency in the tropical tropopause layer: On the interplay
462 between tropical deep convection, large-scale vertical ascent, and horizontal
463 circulations, *J. Geophys. Res.*, 117, D05302, doi:10.1029/2011JD016992, 2012.
- 464 Brewer, A. M.: Evidence for a world circulation provides by the measurements of
465 helium and water vapor distribution in the stratosphere, *Q. J. R. Meteorol. Soc.*,
466 75, 351–363, 1949.
- 467 Cane, M. A., Clement, A. C., Kaplan, A., Kushnir, Y., Pozdnyakov, D., and Seager, R.,
468 et al.: Twentieth-century sea surface temperature trends, *Science*, 275(5302),
469 957-960, DOI: 10.1126/science.275.5302.957, 1997.
- 470 Deser, C., Phillips, A. S., and Alexander, M. A.: Twentieth century tropical sea surface
471 temperature trends revisited, *Geophys. Res. Lett.*, 37(10), L10701,
472 doi:10.1029/2010GL043321, 2010.
- 473 Diallo, M., Ern, M., and Ploeger, F.: The advective Brewer – Dobson circulation in
474 the ERA5 reanalysis: climatology, variability, and trends, *Atmos. Chem. Phys.*,
475 21, 7515 – 7544, <https://doi.org/10.5194/acp-21-7515-2021>, 2021.
- 476 Dobson G. M. B.: Origin and distribution of the polyatomic molecules in the
477 atmosphere, *Proc. R. Soc. Lond. Ser. A*. 236: 187-193, 1956.
- 478 Duncan, B. N., Logan J. A., Bey, I., Megretskaia, I. A., Yantosca, R. M., Novelli, P. C.,
479 Jones, N. B. and Rinsland, C. P.: Global budget of CO, 1988-1997: Source
480 estimates and validation with a global model, *J. Geophys. Res.*, 112, D22301,



- 481 doi:10.1029/2007JD008459, 2007.
- 482 Fueglistaler, S., Desller, A. E., Dunkerton, T. J., Folkins, I., Fu, Q., and Mote P.:
483 Tropical tropopause layer, *Rev. Geophys.*, 47(1), RG1004,
484 doi:10.1029/2008RG000267, 2009.
- 485 Fueglistaler, S., Wernli, H., and Peter, T.: Tropical troposphere-to-stratosphere
486 transport inferred from trajectory calculations, *J. Geophys. Res.*, 109, D03108,
487 doi:10.1029/2003JD004069, 2004.
- 488 Fujiwara, M., Wright, J. S., Manney, G. L., Gray, L. J., Anstey, J., Birner, T., Davis, S.,
489 Gerber, E. P., Harvey, V. L., Hegglin, M. I., Homeyer, C. R., Knox, J. A., Krüger,
490 K., Lambert, A., Long, C. S., Martineau, P., Molod, A., Monge-Sanz, B. M.,
491 Santee, M. L., Tegtmeier, S., Chabrillat, S., Tan, D. G. H., Jackson, D. R.,
492 Polavarapu, S., Compo, G. P., Dragani, R., Ebisuzaki, W., Harada, Y., Kobayashi,
493 C., McCarty, W., Onogi, K., Pawson, S., Simmons, A., Wargan, K., Whitaker, J.
494 S., and Zou, C.-Z.: Introduction to the SPARC Reanalysis Intercomparison
495 Project (S-RIP) and overview of the reanalysis systems, *Atmos. Chem. Phys.*, 17,
496 1417-1452, <https://doi.org/10.5194/acp-17-1417-2017>, 2017
- 497 Garfinkel, C. I., Waugh, D. W., and Polvani, L. M.: Recent Hadley cell expansion:
498 The role of internal atmospheric variability in reconciling modeled and observed
499 trends, *Geophys. Res. Lett.*, 42(24), 10824-10831,
500 <https://doi.org/10.1002/2015GL066942>, 2015
- 501 Garfinkel, C. I., Waugh, D. W., Oman, L. D., Wang, L., and Hurwitz, M. M.:
502 Temperature trends in the tropical upper troposphere and lower stratosphere:
503 Connections with sea surface temperatures and implications for water vapor and
504 ozone, *J. Geophys. Res.*, 118, 9658-9672, doi:10.1002/jgrd.50772, 2013.
- 505 Garfinkel, C. O., Gordon, A., Oman, L. D., Li, F., Davis, S., and Pawson, S.:
506 Nonlinear response of tropical lower-stratospheric temperature and water vapor
507 to ENSO, *Atmos. Chem. Phys.*, 18, 4597-4615,
508 <https://doi.org/10.5194/acp-18-4597-2018>, 2018.
- 509 Gelaro, R., Mccarty, W., and Suárez, M. J.: The modern-era retrospective analysis for
510 research and applications, version 2 (merra-2), *J. Climate*, 30(14), 5419-5454,



- 511 <https://doi.org/10.1175/JCLI-D-16-0758.1>, 2017
- 512 Gettelman, A., Holton, J. R., and Douglass, A. R.: Simulations of water vapor in the
513 lower stratosphere and upper troposphere, *J. Geophys. Res.*, 105(D7), 9003-9023,
514 <https://doi.org/10.1029/1999JD901133>, 2000.
- 515 Gill, A. E.: Some simple solutions for heat-induced tropical circulation, *Q. J. R.*
516 *Meteorolog. Soc.*, 106, 447-462, doi:10.1002/qj.49710644905, 1980.
- 517 Haines, P. E., and Esler, J. G.: Determination of the source regions for surface to
518 stratosphere transport: An Eulerian backtracking approach, *Geophys. Res. Lett.*,
519 41, 1343-1349, doi:10.1002/2013GL058757, 2014.
- 520 Harada, Y., Kamahori, H., Kobayashi, C., Endo, H., Kobayashi, S., Ota, Y., Onoda, H.,
521 Onogi, K., Miyaoka, K., and Takahashi, K.: The JRA-55 Reanalysis:
522 Representation of atmospheric circulation and climate variability, *J. Meteorol.*
523 *Soc. Jpn.*, 94(3), 269-302, <https://doi.org/10.2151/jmsj.2016-015>, 2016.
- 524 Hersbach, H., Bell, B., Berrisford, P., Hirahara, S., Horányi, A., Muñoz-Sabater, J.,
525 and Nicolas, J., et al.: The ERA5 global reanalysis, *Q. J. R. Meteorol. Soc.*, 146,
526 1999-2049, DOI: 10.1002/qj.3803, 2020.
- 527 Highwood, E. J., and Hoskins, B. J.: The tropical tropopause, *Q. J. R. Meteorol. Soc.*,
528 124(549), 1579-1604, DOI: 10.1002/qj.49712454911, 1998.
- 529 Hitchcock, P.: On the value of reanalyses prior to 1979 for dynamical studies of
530 stratosphere-troposphere coupling, *Atmos. Chem. Phys.*, 19, 2749-2764,
531 <https://doi.org/10.5194/acp-19-2749-2019>, 2019
- 532 Holton, J. R., Haynes, P. H., McIntyre, M. E., Douglass, A. R., Rood, R. B., and
533 Pfister, L.: Stratosphere-troposphere exchange, *Rev. Geophys.*, 33,
534 403-439, <https://doi.org/10.1029/95RG02097>, 1995.
- 535 Hosking, J. S., Russo, M. R., Braesicke, P., and Pyle, J. A.: Tropical convective
536 transport and the Walker circulation, *Atmos. Chem. Phys.*, 12, 9791-9797,
537 doi:10.5194/acp-12-9791-2012, 2012
- 538 Hu, D., Tian, W., Guan, Z., Guo, Y., and Dhomse, S.: Longitudinal asymmetric trends
539 of tropical cold-point tropopause temperature and their link to strengthened
540 Walker circulation, *J. Climate*, 29(21), 7755-7771,



- 541 <https://doi.org/10.1175/JCLI-D-15-0851.1>, 2016.
- 542 Hu, P., Huangfu, J., Chen, W., and Huang, R.: Impacts of early/late South China Sea
543 summer monsoon withdrawal on tropical cyclone genesis over the western North
544 Pacific, *Clim. Dynam.*, 55(19), 1507-1520,
545 <https://doi.org/10.1007/s00382-020-05339-7>, 2020.
- 546 Kobayashi, S., Ota, Y., Harada, Y., Ebata, A., Moriya, M., and Onoda, H., et al.: The
547 JRA-55 Reanalysis: General specifications and basic characteristics, *J. Meteorol.*
548 *Soc. Jpn.*, 93, 5-48, DOI:10.2151/jmsj.2015-001, 2015.
- 549 Krüger, K., Tegtmeier, S., and Rex, M.: Long-term climatology of air mass transport
550 through the Tropical Tropopause Layer (TTL) during NH winter, *Atmos. Chem.*
551 *Phys.*, 8, 813–823, doi:10.5194/acpd-7-13989-2007, 2008.
- 552 L'Heureux, M. L., Lee, S., and Lyon, B.: Recent multidecadal strengthening of the
553 Walker circulation across the tropical Pacific, *Nat. Clim. Change*, 3, 571–576,
554 doi: 10.1038/nclimate1840, 2013.
- 555 Levine, J. G., Braesicke, P., Harris, N. R. P., Pyle, J. A.: Seasonal and inter-annual
556 variations in troposphere-to-stratosphere transport from the tropical tropopause
557 layer, *Atmos. Chem. Phys.*, 8, 3689-3703, DOI:10.5194/acpd-8-489-2008, 2008.
- 558 Levine, J. G., Braesicke, P., Harris, N. R. P., Savage, N. H., and Pyle, J. A.: Pathways
559 and timescales for troposphere-to-stratosphere transport via the tropical
560 tropopause layer and their relevance for very short lived substances, *J. Geophys.*
561 *Res.*, 112, D04308, doi:10.1029/2005JD006940, 2007.
- 562 Liebmann, B., and Smith, C. A.: Description of a complete (interpolated) outgoing
563 longwave radiation dataset, *B. Am. Meteorol. Soc.*, 77, 1275-1277, doi:
564 10.1175/1520-0477(1996)077<1255:EA>2.0.CO;2, 1996.
- 565 Lin, P., Ming, Y., and Ramaswamy, V.: Tropical climate change control of the lower
566 stratospheric circulation, *Geophys. Res. Lett.*, 42(3), 941-948, doi:
567 10.1002/2014GL062823, 2015.
- 568 Logan, J. A., Megretskaia, I. A., Nassar, R., Murray, L. T., Zhang, L., Bowman, K. W.,
569 Worden, H. M., and Luo, M.: Effects of the 2006 El Niño on tropospheric
570 composition as revealed by data from the Tropospheric Emission Spectrometer



- 571 (TES), *Geophys. Res. Lett.*, 35, L03816,
572 <https://doi.org/10.1029/2007GL031698>, 2008.
- 573 Lu, J., Vecchi, G. A., and Reichler, T.: Expansion of the Hadley cell under global
574 warming, *Geophys. Res. Lett.*, 34(6), L06805, doi:10.1029/2006GL028443,
575 2007
- 576 Lu, J., Xie, F., Sun, C., Luo, J., Cai, Q., Zhang, J., Li, J., and Tian, H.: Analysis of
577 factors influencing tropical lower stratospheric water vapor during 1980–2017,
578 *npj Clim. Atmos. Sci.*, 3(1), 35, <https://doi.org/10.1038/s41612-020-00138-7>,
579 2020.
- 580 Ma, S., and Zhou, T.: Robust Strengthening and Westward Shift of the Tropical
581 Pacific Walker Circulation during 1979–2012: A Comparison of 7 Sets of
582 Reanalysis Data and 26 CMIP5 Models, *J. Climate*, 29, 3097–3118, doi:
583 10.1175/JCLI-D-15-0398.1, 2016.
- 584 Marsh, D. R., Mills, M. J., Kinnison, D. E., Lamarque, J., Calvo, N., and Polvani, L.
585 M.: Climate change from 1850 to 2005 simulated in CESM1 (WACCM), *J.*
586 *Climate*, 26, 7372–7391, <https://doi.org/10.1175/JCLI-D-12-00558.1>, 2013.
- 587 McGregor, S., Timmermann, A., Stuecker, M. F., England, M. H., Merrifield, M., Jin,
588 F., and Chikamoto, Y.: Recent Walker circulation strengthening and Pacific
589 cooling amplified by Atlantic warming, *Nat. Clim. Change*, 4, 888–882,
590 <https://doi.org/10.1038/nclimate2330>, 2014.
- 591 Meng, Q., Latif, M., Park, W., Keenlyside, N. S., Semenov, V. A., and Martin, T.:
592 Twentieth century Walker circulation change: Data analysis and model
593 experiments, *Clim. Dynam.*, 38, 1757–1773,
594 <https://doi.org/10.1007/s00382-011-1047-8>, 2012.
- 595 Navarro, M. A., Atlas, E. L., Saiz-Lopez, A., Rodriguez-Lloveras, X., Kinnison, D. E.,
596 Lamarque, J., Tilmes, S., Filus, M., and Harris, N. R. P., et al.: Airborne
597 measurements of organic bromine compounds in the Pacific tropical tropopause
598 layer, *P. Natl. Acad. Sci. USA*, 112, 13789–13793, doi:10.1073/pnas.1511463112,
599 2015.
- 600 Newell, R. E., and Gould-Stewart, S.: A stratospheric fountain? *J. Atmos. Sci.*, 38,



- 601 2789–2796, DOI: 10.1175/1520-0469(1981)038<2789:ASF>2.0.CO;2, 1981.
- 602 Newton, R., Vaughan, G., Hints, E., Filus, M. T., Pan, L. L., and Homomichl, S., et al.:
- 603 Observations of ozone-poor air in the tropical tropopause layer, *Atmos. Chem.*
- 604 *Phys.*, 18, 5157–5171, <https://doi.org/10.5194/acp-18-5157-2018>, 2018.
- 605 Pan, L. L., Atlas, E. L., Salawitch, R. J., Homomichl, S. B., Bresch, J. F., and Randel,
- 606 W. J., et al.: The Convective Transport of Active Species in the Tropics
- 607 (CONTRAST) Experiment, *B. Am. Meteorol. Soc.*, 98(1), 106–128,
- 608 DOI: 10.1175/BAMS-D-14-00272.1, 2016.
- 609 Pan, L. L., Homomichl, S. B., Thornberry, T., Rollins, A., Bui, T. P., Pfister, L., and
- 610 Jensen E. E.: Observational Evidence of Horizontal Transport-Driven
- 611 Dehydration in the TTL, *Geophys. Res. Lett.*, 46(13), 7848–7856,
- 612 DOI: 10.1029/2019GL083647, 2019
- 613 Randel, W. J., and Jensen, E. J.: Physical processes in the tropical tropopause layer
- 614 and their roles in a changing climate, *Nat. Geosci.*, 6, 169–176,
- 615 DOI:10.1038/ngeo1733, 2013.
- 616 Rao, J., Yu, Y., Guo, D., Shi, C., Chen, D., and Hu, D.: Evaluating the Brewer-Dobson
- 617 circulation and its responses to ENSO, QBO, and the solar cycle in different
- 618 reanalyses, *Earth Planet. Phys.*, 3(2), 1–16, <http://doi.org/10.26464/epp2019012>,
- 619 2019.
- 620 Rayner, N., Parker, D., Horton, E., Folland, C. K., Alexander, L., and Rowell, D. P., et
- 621 al.: Global analyses of sea surface temperature, sea ice, and night marine air
- 622 temperature since the late nineteenth century, *J. Geophys. Res.*, 108(D14), 4407,
- 623 doi:10.1029/2002JD002670, 2003.
- 624 Rosenlof, K. H. How water enters the stratosphere, *Science*, 302, 1691–1692,
- 625 doi:10.1126/science.1092703, 2003.
- 626 Ryu, J., and Lee, S.: Effect of tropical waves on the tropical tropopause transition
- 627 layer upwelling, *J. Atmos. Sci.*, 67(10), 3130–3148,
- 628 DOI: 10.1175/2010JAS3434.1, 2010.
- 629 Saiz-Lopez, A., and von Glasow, R.: Reactive halogen chemistry in the troposphere,
- 630 *Chem. Soc. Rev.*, 41, 6448–6472, DOI:10.1039/c2cs35208g, 2012.



- 631 Schoeberl, M. R., Jensen, E. J., Pfister, L., Ueyama, R., Avery, M., and Dessler, A. E.:
632 Convective hydration of the upper troposphere and lower stratosphere, *J.*
633 *Geophys. Res.*, 123(9), 4583-4593, <https://doi.org/10.1029/2018JD028286>, 2018.
- 634 Sherwood, S. C.: A stratospheric “drain” over the maritime continent, *Geophys. Res.*
635 *Lett.*, 27(5), 677-680, <https://doi.org/10.1029/1999GL010868>, 2000.
- 636 Tokinaga, H., Xie, S. P., Deser, C., Kosaka, Y., and Okumura, Y. M.: Slowdown of the
637 Walker circulation driven by tropical Indo-Pacific warming. *Nature*, 491,
638 439–443, DOI: 10.1038/nature11576, 2012.
- 639 Uma, K. N., Das, S. S., Ratnam, M. V., and Suneeth, K. V.: Assessment of vertical air
640 motion among reanalyses and qualitative comparison with very-high-frequency
641 radar measurements over two tropical stations, *Atmos. Chem. Phys.*, 21,
642 2083-2103, <https://doi.org/10.5194/acp-21-2083-2021>, 2021.
- 643 Wales, P. A., Salawitch, R. J., Nicely, J. M., Anderson, D. C., Canty, T. P. and Baidar,
644 S., et al.: Stratospheric injection of Brominated very short-lived substances:
645 Aircraft observations in the western Pacific and representation in global models,
646 *J. Geophys. Res.*, 123(10), 5690-5719, <https://doi.org/10.1029/2017JD027978>,
647 2017.
- 648 Wang, S., Schmidt, J. A., Baidar, S., Coburn, S., Dix, B., and Koenig, T. K., et al.:
649 Active and wide-spread halogen chemistry in the tropical and subtropical free
650 troposphere, *P. Natl. Acad. Sci. USA*, 112, 9281–9286,
651 DOI: 10.1073/pnas.1505142112, 2015.
- 652 Wang, W., Matthes, K., and Schmidt, T.: Quantifying contributions to the recent
653 temperature variability in the tropical tropopause layer, *Atmos. Chem. Phys.*, 15,
654 5815–5826, doi:10.5194/acp-15-5815-2015, 2015.
- 655 Wang, W., Matthes, K., Omarani, N.-E., and Latif, M.: Decadal variability of tropical
656 tropopause temperature and its relationship to the Pacific Decadal Oscillation,
657 *Sci. Rep.*, 6, 29537, <https://doi.org/10.1038/srep29537>, 2016.
- 658 Webster, P. J., Lukas, R.: TOGA COARE: the coupled ocean-atmosphere response
659 experiment, *B. Am. Meteorol. Soc.*, 73(9), 1377-1416,
660 DOI: 10.1175/1520-0477(1992)073<1377:TCTCOR>2.0.CO;2, 1992.



- 661 Webster, P. J., Clayson, C. A., Curry, J. A.: Clouds, radiation, and the diurnal cycle of
662 sea surface temperature in the tropical western Pacific, *J. Climate*, 8(8),
663 1712-1730, DOI: 10.1175/1520-0442(1996)009<1712:CRATDC>2.0.CO;2,
664 1996.
- 665 Xie, F., Li, J., Tian, W., Feng, J., and Huo, Y.: Signals of El Niño Modoki in the
666 tropical tropopause layer and stratosphere, *Atmos. Chem. Phys.*, 12, 5259-5273,
667 doi:10.5194/acp-12-5259-2012, 2012.
- 668 Xie, F., Li, J., Tian, W., Li, Y., and Feng, J.: Indo-Pacific Warm Pool Area Expansion,
669 Modoki Activity, and Tropical Cold-Point Tropopause Temperature Variations,
670 *Sci. Rep.*, 4, 4552, <https://doi.org/10.1038/srep04552>, 2014a.
- 671 Xie, F., Li, J., Tian, W., Zhang, J., and Shu, J.: The impacts of two types of El Niño on
672 global ozone variations in the last three decades, *Adv. Atmos. Sci.*, 31(5),
673 1113-1126, doi: 10.1007/s00376-013-3166-0, 2014b.
- 674 Xie, F., Tian, W., Zhou, X., Zhang, J., Xia, Y., and Lu, J.: Increase in lower
675 stratospheric water vapor in the past 100 years related to tropical Atlantic
676 warming, *Geophys. Res. Lett.*, 47, e2020GL090539,
677 DOI: 10.1029/2020GL090539, 2020.
- 678 Zhou, X., Chen, Q., Li, Y., Zhao, Y., Lin, Y., and Jiang, Y.: Impacts of the Indo-Pacific
679 warm pool on lower stratospheric water vapor: Seasonality and hemispheric
680 contrasts, *J. Geophys. Res.*, 126, e2020JD034363, DOI: 10.1029/2020JD034363,
681 2021.

682

683 **Figure captions:**

684 **Fig. 1.** The climatological mean (averaged over 1958-2017) values of 150 hPa w (10^{-2}
685 m s^{-1}) in different months using the JRA55 reanalysis data.

686 **Fig. 2.** The trends of (a) 150 hPa horizontal winds (arrows, units: $10^{-1} \text{ m s}^{-1} \text{ a}^{-1}$) and
687 vertical velocity (shading, units: $10^{-4} \text{ m s}^{-1} \text{ a}^{-1}$); (d) 500 hPa horizontal winds (arrows,
688 units: $10^{-1} \text{ m s}^{-1} \text{ a}^{-1}$) and vertical velocity (shading, units: $10^{-4} \text{ m s}^{-1} \text{ a}^{-1}$); and (g) 700



689 hPa horizontal winds (arrows, units: $10^{-1} \text{ m s}^{-1} \text{ a}^{-1}$) and vertical velocity (shading, units:
690 $10^{-4} \text{ m s}^{-1} \text{ a}^{-1}$) from JRA55 in NDJFM during 1958-2017. (b), (e), and (h) are the same
691 as (a), (d), and (g) but for ERA5. (c), (f) and (i) are the same as (a), (d), and (g) except
692 that the trends are during 1980-2017 and the wind field data are from MERRA2. The
693 vertical velocity trends over the dotted regions are statistically significant at the 95%
694 confidence level. The white areas denote missing values.

695 **Fig. 3.** The time series of the standardized intensity of the upward motion over the
696 tropical western Pacific (20°S - 10°N , 100°E - 180°E) at (a) 150 hPa; (b) 500 hPa; and
697 (c) 700 hPa extracted from JRA55 (red), ERA5 (black) and MERRA2 (blue) datasets.
698 The straight lines in each figure indicates the linear trends. The linear trends of the
699 upward motion intensity over the TWP at all levels from three datasets are statistically
700 significant at the 90% confidence level.

701 **Fig. 4.** Trends of (a) outgoing longwave radiation (OLR, units: $\text{W m}^{-2} \text{ a}^{-1}$) during
702 1974-2017; (b) cold-point tropopause temperature (CPTT, units: 10^{-1} K a^{-1}) and (c)
703 SST (K a^{-1}) during 1958-2017 in NDJFM. (d) The correlation coefficients between the
704 intensity of the upward motion at 150 hPa over the TWP and SST with the linear
705 trends removed. The trends and correlation coefficients over the dotted regions are
706 statistically significant at the 95% confidence level.

707 **Fig. 5.** The trends of 150 hPa w (shading, units: $10^{-4} \text{ m s}^{-1} \text{ a}^{-1}$) and horizontal winds
708 (arrows; $10^{-1} \text{ m s}^{-1} \text{ a}^{-1}$) from (a) Control run; (b) Fixsst run; and (c) difference between
709 the Control run and the Fixsst run in NDJFM during 1958-2017. (d)-(f) are similar to
710 (a)-(c) but for 500 hPa horizontal winds (arrows, units: $10^{-1} \text{ m s}^{-1} \text{ a}^{-1}$) and vertical



711 velocity (shading, units: $10^{-4} \text{ m s}^{-1} \text{ a}^{-1}$). (g)-(i) are similar to (d)-(f) but for 700 hPa
712 horizontal winds (arrows, units: $10^{-1} \text{ m s}^{-1} \text{ a}^{-1}$) and vertical velocity (shading, units:
713 $10^{-4} \text{ m s}^{-1} \text{ a}^{-1}$). The vertical velocity trends over the dotted regions are statistically
714 significant at the 95% confidence level.

715 **Fig. 6.** The difference between two time-slice simulations (R1 and R2). Differences of
716 (a) 150 hPa w (shading, units: 10^{-2} m s^{-1}) and horizontal winds (arrows, units: m s^{-1});
717 (b) 500 hPa w (shading, units: 10^{-2} m s^{-1}) and horizontal winds (arrows, units: m s^{-1});
718 (c) 700 hPa w (shading, units: 10^{-2} m s^{-1}) and horizontal winds (arrows, units: m s^{-1}) in
719 NDJFM. The differences between vertical velocity over the dotted regions are
720 statistically significant at the 95% confidence level.

721 **Fig. 7.** The trends of outgoing longwave radiation (OLR; units: $\text{W m}^{-2} \text{ a}^{-1}$) from (a)
722 Control run; (b) Fixsst run; and (c) difference between the Control run and the Fixsst
723 run in NDJFM during 1958-2017. (d)-(f) are similar to (a)-(c) but for CPTT (shading,
724 units: 10^{-1} K a^{-1}) and 100 hPa streamfunction (contour, units: $10^6 \text{ m}^2 \text{ s}^{-1} \text{ a}^{-1}$). (g)-(i) are
725 similar to (d)-(f) but for 70 hPa water vapor concentration (units: $10^{-2} \text{ ppmv a}^{-1}$). The
726 trends in (a)-(c) and (g)-(i) over the dotted regions are statistically significant at the
727 95% confidence level. The CPTT trends in (d)-(f) over the dotted regions are
728 statistically significant at the 95% confidence level.

729 **Fig. 8.** The trends of 150 hPa CO concentration ($10^{-4} \text{ ppmv a}^{-1}$) from (a) Control run;
730 (b) Fixsst run; and (c) difference between the Control run and the Fixsst run in
731 NDJFM during 1958-2017. The trends in (a)-(c) over the dotted regions are
732 statistically significant at the 95% confidence level.



733 **Fig. 9.** Latitude-pressure cross sections of the trends of the zonal mean CO
734 concentration (10^{-4} ppmv a^{-1}) from (a) Control run; (b) Fixsst run; and (c) difference
735 between the Control run and the Fixsst run in NDJFM during 1958-2017. (d)-(f) are
736 the same as (a)-(c) but for the CO concentration averaged over the TWP
737 (100°E - 180°E). The trends over the dotted regions are statistically significant at the
738 95% confidence level.

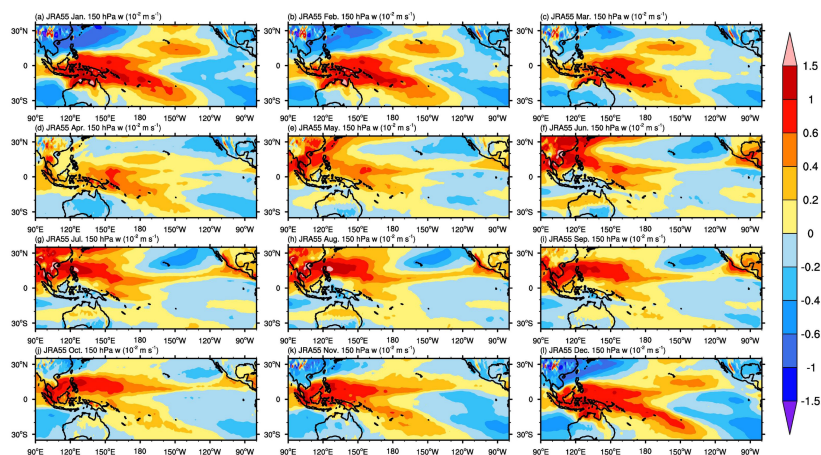
739 **Fig. 10.** Latitude-pressure cross sections of the trends of the zonal mean w (10^{-4} m s^{-1}
740 a^{-1}) and v (10^{-1} $\text{m s}^{-1} a^{-1}$) from (a) Control run; (b) Fixsst run; and (c) difference
741 between the Control run and the Fixsst run in NDJFM during 1958-2017. (d)-(f) are
742 similar to the (a)-(c) but for the trends of the w (10^{-4} $\text{m s}^{-1} a^{-1}$) and v (10^{-1} $\text{m s}^{-1} a^{-1}$)
743 over the TWP (100°E - 180°E). The shadings denote the trends of the w (10^{-4} $\text{m s}^{-1} a^{-1}$).
744 The trends over the dotted regions are statistically significant at the 90% confidence
745 level.

746 **Fig. 11.** Latitude-pressure cross sections of the trends of the BD circulation (vectors,
747 units in the horizontal and vertical components are 10^{-2} and 10^{-5} $\text{m s}^{-1} a^{-1}$, respectively)
748 from (a) Control run; (b) Fixsst run; (c) difference between the Control run and the
749 Fixsst run; and (d) JRA55. The shadings are the trends of the vertical velocities (10^{-5}
750 $\text{m s}^{-1} a^{-1}$). The trends of the vertical velocity over the dotted regions are statistically
751 significant at the 90% confidence level.

752



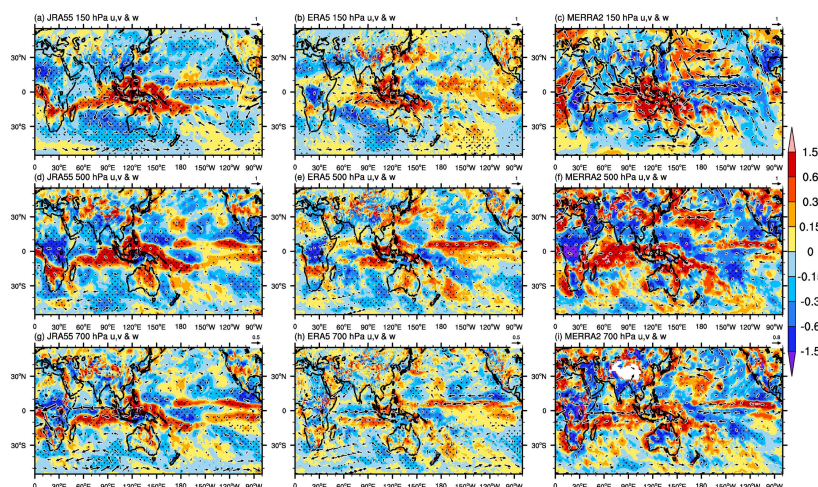
753 **Figures**



754

755 **Fig. 1.** The climatological mean (averaged over 1958-2017) values of 150 hPa w (10^{-2}
756 m s^{-1}) in different months using the JRA55 reanalysis data.

757



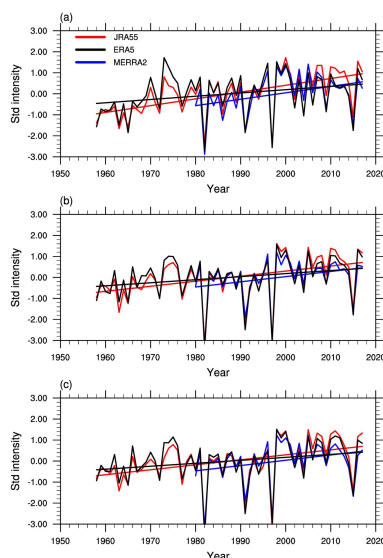
758

759 **Fig. 2.** The trends of (a) 150 hPa horizontal winds (arrows, units: $10^{-1} \text{ m s}^{-1} \text{ a}^{-1}$) and
760 vertical velocity (shading, units: $10^{-4} \text{ m s}^{-1} \text{ a}^{-1}$); (d) 500 hPa horizontal winds (arrows,
761 units: $10^{-1} \text{ m s}^{-1} \text{ a}^{-1}$) and vertical velocity (shading, units: $10^{-4} \text{ m s}^{-1} \text{ a}^{-1}$); and (g) 700
762 hPa horizontal winds (arrows, units: $10^{-1} \text{ m s}^{-1} \text{ a}^{-1}$) and vertical velocity (shading, units:
763 $10^{-4} \text{ m s}^{-1} \text{ a}^{-1}$) from JRA55 in NDJFM during 1958-2017. (b), (e), and (h) are the same
764 as (a), (d), and (g) but for ERA5. (c), (f) and (i) are the same as (a), (d), and (g) except
765 that the trends are during 1980-2017 and the wind field data are from MERRA2. The
766 vertical velocity trends over the dotted regions are statistically significant at the 95%
767 confidence level. The white areas denote missing values.

768



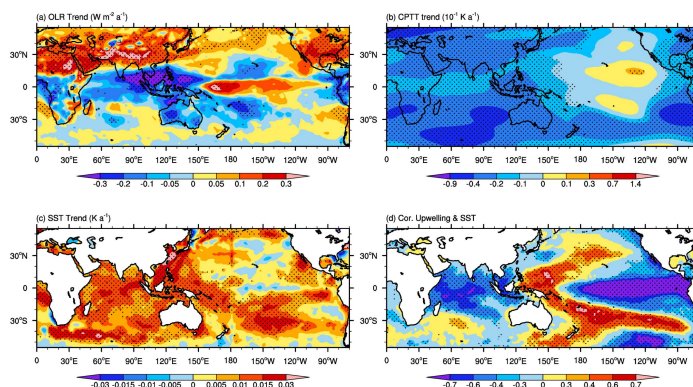
769



770

771 **Fig. 3.** The time series of the standardized intensity of the upward motion over the
772 tropical western Pacific (20°S - 10°N , 100°E - 180°E) at (a) 150 hPa; (b) 500 hPa; and
773 (c) 700 hPa extracted from JRA55 (red), ERA5 (black) and MERRA2 (blue) datasets.
774 The straight lines in each figure indicates the linear trends. The linear trends of the
775 upward motion intensity over the TWP at all levels from three datasets are statistically
776 significant at the 90% confidence level.

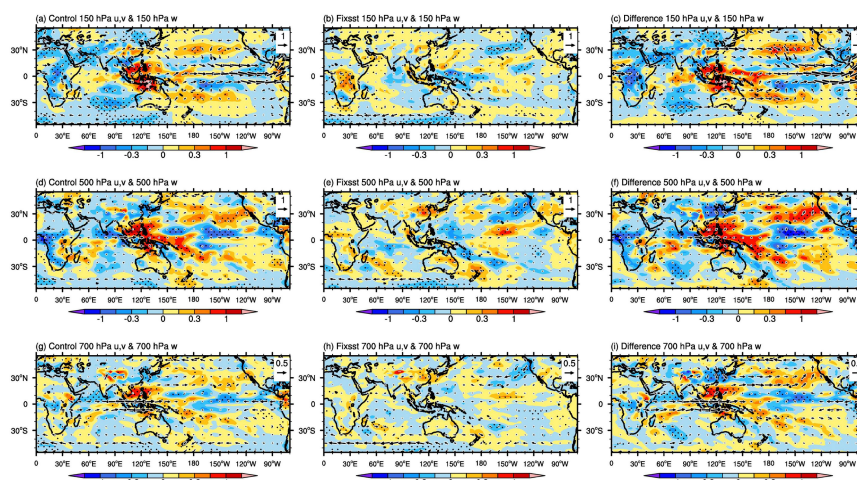
777



778

779 **Fig. 4.** Trends of (a) outgoing longwave radiation (OLR, units: $\text{W m}^{-2} \text{ a}^{-1}$) during
780 1974-2017; (b) cold-point tropopause temperature (CPTT, units: 10^{-1} K a^{-1}) and (c)
781 SST (K a^{-1}) during 1958-2017 in NDJFM. (d) The correlation coefficients between the
782 intensity of the upward motion at 150 hPa over the TWP and SST with the linear
783 trends removed. The trends and correlation coefficients over the dotted regions are
784 statistically significant at the 95% confidence level.

785



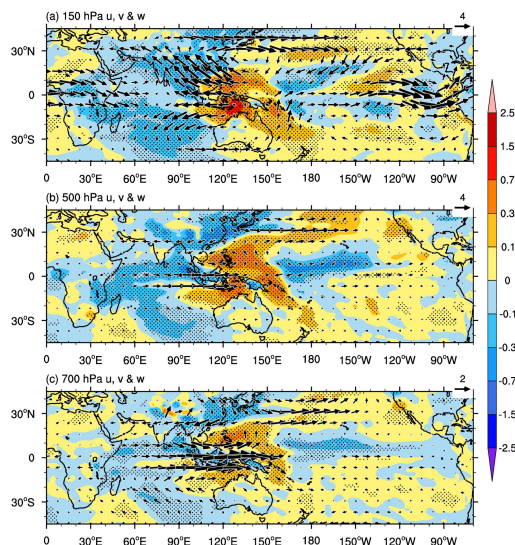
786

787 **Fig. 5.** The trends of 150 hPa w (shading, units: $10^{-4} \text{ m s}^{-1} \text{ a}^{-1}$) and horizontal winds
788 (arrows; $10^{-1} \text{ m s}^{-1} \text{ a}^{-1}$) from (a) Control run; (b) Fixsst run; and (c) difference between
789 the Control run and the Fixsst run in NDJFM during 1958-2017. (d)-(f) are similar to
790 (a)-(c) but for 500 hPa horizontal winds (arrows, units: $10^{-1} \text{ m s}^{-1} \text{ a}^{-1}$) and vertical
791 velocity (shading, units: $10^{-4} \text{ m s}^{-1} \text{ a}^{-1}$). (g)-(i) are similar to (d)-(f) but for 700 hPa
792 horizontal winds (arrows, units: $10^{-1} \text{ m s}^{-1} \text{ a}^{-1}$) and vertical velocity (shading, units:
793 $10^{-4} \text{ m s}^{-1} \text{ a}^{-1}$). The vertical velocity trends over the dotted regions are statistically
794 significant at the 95% confidence level.

795



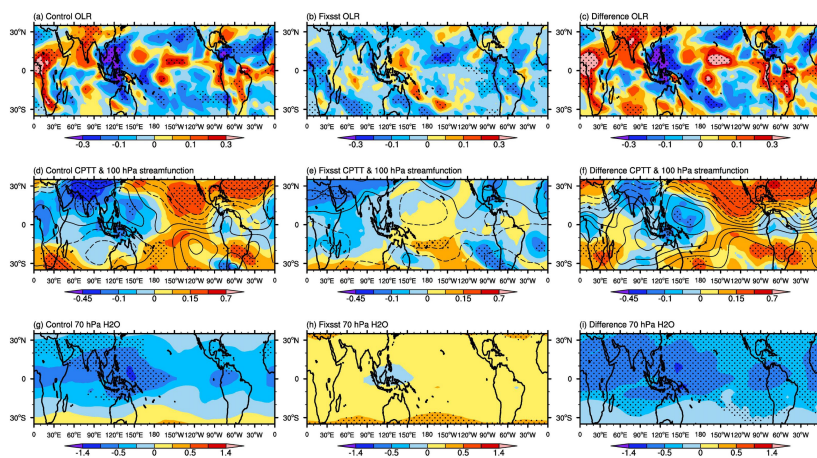
796



797

798 **Fig. 6.** The difference between two time-slice simulations (R1 and R2). Differences of
799 (a) 150 hPa w (shading, units: 10^{-2} m s^{-1}) and horizontal winds (arrows, units: m s^{-1});
800 (b) 500 hPa w (shading, units: 10^{-2} m s^{-1}) and horizontal winds (arrows, units: m s^{-1});
801 (c) 700 hPa w (shading, units: 10^{-2} m s^{-1}) and horizontal winds (arrows, units: m s^{-1}) in
802 NDJFM. The differences between vertical velocity over the dotted regions are
803 statistically significant at the 95% confidence level.

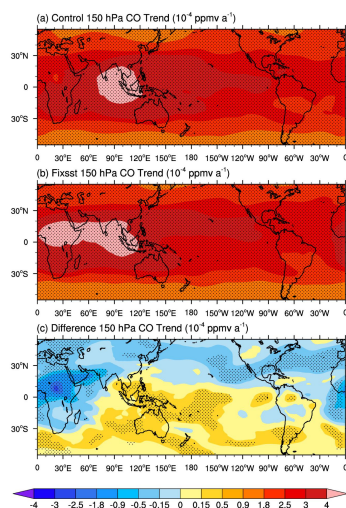
804



805

806 **Fig. 7.** The trends of outgoing longwave radiation (OLR; units: $\text{W m}^{-2} \text{a}^{-1}$) from (a)
807 Control run; (b) Fixsst run; and (c) difference between the Control run and the Fixsst
808 run in NDJFM during 1958-2017. (d)-(f) are similar to (a)-(c) but for CPTT (shading,
809 units: 10^{-1}K a^{-1}) and 100 hPa streamfunction (contour, units: $10^6 \text{m}^2 \text{s}^{-1} \text{a}^{-1}$). (g)-(i) are
810 similar to (d)-(f) but for 70 hPa water vapor concentration (units: $10^{-2} \text{ppmv a}^{-1}$). The
811 trends in (a)-(c) and (g)-(i) over the dotted regions are statistically significant at the
812 95% confidence level. The CPTT trends in (d)-(f) over the dotted regions are
813 statistically significant at the 95% confidence level.

814



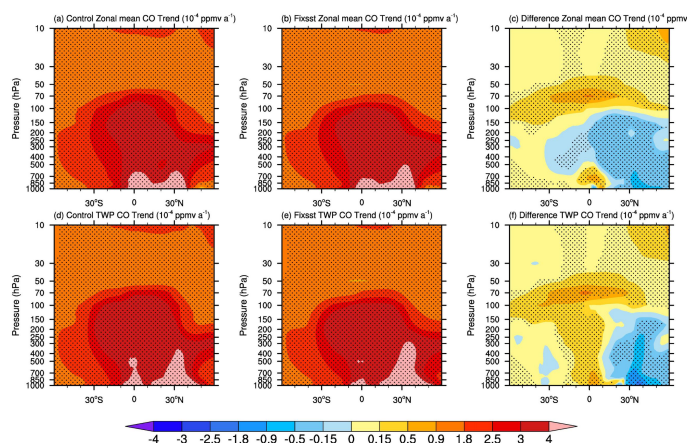
815

816 **Fig. 8.** The trends of 150 hPa CO concentration (10^{-4} ppmv a⁻¹) from (a) Control run;
817 (b) Fixsst run; and (c) difference between the Control run and the Fixsst run in
818 NDJFM during 1958-2017. The trends in (a)-(c) over the dotted regions are
819 statistically significant at the 95% confidence level.

820



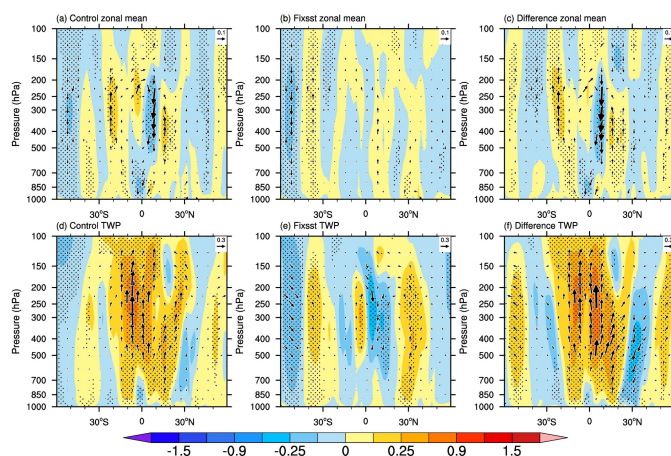
821



822

823 **Fig. 9.** Latitude-pressure cross sections of the trends of the zonal mean CO
824 concentration (10^{-4} ppmv a^{-1}) from (a) Control run; (b) Fixsst run; and (c) difference
825 between the Control run and the Fixsst run in NDJFM during 1958-2017. (d)-(f) are
826 the same as (a)-(c) but for the CO concentration averaged over the TWP
827 (100°E - 180°E). The trends over the dotted regions are statistically significant at the
828 95% confidence level.

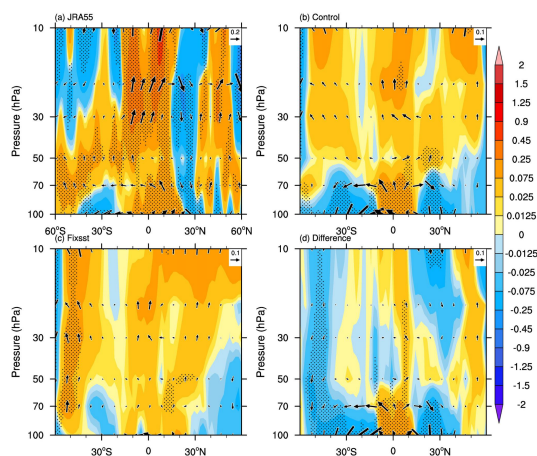
829



830

831 **Fig. 10.** Latitude-pressure cross sections of the trends of the zonal mean w (10^{-4} m s^{-1}
832 a^{-1}) and v ($10^{-1} \text{ m s}^{-1} \text{ a}^{-1}$) from (a) Control run; (b) Fixsst run; and (c) difference
833 between the Control run and the Fixsst run in NDJFM during 1958-2017. (d)-(f) are
834 similar to the (a)-(c) but for the trends of the w ($10^{-4} \text{ m s}^{-1} \text{ a}^{-1}$) and v ($10^{-1} \text{ m s}^{-1} \text{ a}^{-1}$)
835 over the TWP (100°E - 180°E). The shadings denote the trends of the w ($10^{-4} \text{ m s}^{-1} \text{ a}^{-1}$).
836 The trends over the dotted regions are statistically significant at the 90% confidence
837 level.

838



839

840 **Fig. 11.** Latitude-pressure cross sections of the trends of the BD circulation (vectors,
841 units in the horizontal and vertical components are 10^{-2} and $10^{-5} \text{ m s}^{-1} \text{ a}^{-1}$, respectively)
842 from (a) Control run; (b) Fixsst run; (c) difference between the Control run and the
843 Fixsst run; and (d) JRA55. The shadings are the trends of the vertical velocities (10^{-5}
844 $\text{ m s}^{-1} \text{ a}^{-1}$). The trends of the vertical velocity over the dotted regions are statistically
845 significant at the 90% confidence level.

846